First-principles calculation of the structural stability of 6*d* transition metals

A. Östlin[1,*] and L. Vitos[1,2,3]

[1]*Department of Materials Science and Engineering, Applied Materials Physics, KTH Royal Institute of Technology, Stockholm SE-100 44, Sweden*

[2]*Department of Physics and Materials Science, Uppsala University, P.O. Box 516, SE-75120 Uppsala, Sweden*

[3]*Research Institute for Solid State Physics and Optics, P.O. Box 49, H-1525 Budapest, Hungary*

(Received 30 June 2011; revised manuscript received 18 August 2011; published 13 September 2011)

The phase stability of the 6*d* transition metals (elements 103–111) is investigated using first-principles electronic-structure calculations. Comparison with the lighter transition metals reveals that the structural sequence trend is broken at the end of the 6*d* series. To account for this anomalous behavior, the effect of relativity on the lattice stability is scrutinized, taking different approximations into consideration. It is found that the mass-velocity and Darwin terms give important contributions to the electronic structure, leading to changes in the interstitial charge density and, thus, in the structural energy difference.

DOI: 10.1103/PhysRevB.84.113104 PACS number(s): 71.15.Rf, 71.15.Nc, 71.20.Be, 81.05.Bx

One of the characteristic properties of solid materials is the crystal structure. The thermodynamically most stable structure for a given solid has been predicted with good accuracy over the years by using different density functional theory (DFT)[1,2] schemes. The common procedure used is to calculate the equation of state of different competing crystal structures, and then the most stable state at ambient pressure is the one that possesses the lowest total energy. Nonmagnetic transition metals crystallize in three kinds of close-packed structures: hexagonal-close-packed (hcp) structures, face-centered-cubic (fcc) structures, and body-centered-cubic (bcc) structures, and they follow the general hcp-bcc-hcp-fcc structural sequence as one progresses from group 3 toward group 11. In magnetic 3*d* metals, magnetism leads to decoupling of bands of different spin, which in turn, dictates a different structural variety.[3]

The conventional explanation for the normal structural sequence can be found by considering the *d*-electron occupation and the shape of the density of states (DOS).[4] In transition metals, the valence part of the DOS can be separated into two parts, one narrow *d* part superimposed on a relatively broad part from the *sp*-like states. The shape of the *d* part, in general, can be explained from the so-called *canonical band theory*, which only takes the structure into consideration but not the atomic type. From this picture, the lattice stability of a transition metal can be thought of as a competition between the kinetic (one-electron) energy, which favors structures with low DOS near the Fermi level and the electrostatic (Madelung) interaction favoring the high-symmetry structures.[5]

In recent years, electronic-structure calculations have been performed for elements heavier than the actinides.[6–8] Even if these elements have never been synthesized in macroscopic samples big enough for experimental probing of crystal structure, it is only natural to ask if the accepted theories still hold for the heavier transition metals. One particularly important question is the role of relativistic terms. In heavy elements, relativistic effects could have a large impact, since their strength increases with increasing nuclear charge. In common electronic-structure studies, the effect of relativity is taken into account within the so-called scalar-relativistic (SR) approximation. According to that, the mass-velocity term and the Darwin term are treated properly while the more complicated spin-orbit (SO) term is neglected. If the SO term is to be considered, it can be treated either as a perturbation or by solving the four-component Dirac equation. The latter is usually referred to as the fully relativistic (FR) treatment.

This Brief Report aims to investigate the structural sequence in the case of the 6*d* transition metals (Table I), taking the relativistic effects into particular consideration. The calculations were performed using DFT implemented within the exact-muffin-tin-orbitals (EMTO) method[10–13] and the local-density approximation (LDA).[14] The reason for this choice is that, according to previous studies on the equilibrium properties of transition metals,[11,15] the LDA performs somewhat better for the heavy transition metals compared to the common gradient level approximations. For the bcc, fcc, and hcp lattices 285, 240, and 539, respectively, uniformly distributed **k**-points were used in the irreducible Brillouin zone. For the muffin-tin orbitals, an $spdf$ basis ($\ell_{\max} = 3$) was adopted. Increasing the basis set to $spdfgh$ ($\ell_{\max} = 5$) gave a change in total energy of 1 mRy and a decrease in the Wigner-Seitz radius of 0.02 Bohr. Accordingly, we set out error bars at 1 mRy in the structural energy difference and at 0.02 Bohr in the Wigner-Seitz radius. The Green's function was calculated on a semicircular contour using complex energy points distributed exponentially. For the slope matrix, we employed the two-center Taylor expansion.[16] The contour integration depth ranged from 2.5 Ry (below the Fermi level) for the early 6*d* metals (Lr, Rf, and Db) to 1.0 Ry for Sg and 1.5 Ry for the latter metals (Bh, Hs, Mt, Ds, and Rg). For the 2.5-Ry contours, 36 energy points were used, while 21 points were used for the remaining contours. For elements 103–105, the $5f$, $6p$, $6d$, and $7s$ states and, for the rest of the elements, the $6d$ and $7s$ states were treated as valence states. To be able to discern the effect of relativity, the EMTO method was applied using a SR and a nonrelativistic (NR) approximation as well as a FR calculation (solving the four-component Dirac equation). In all these three cases, the core states were treated as FR and were relaxed during the self-consistent iterations.

For comparison, in addition to the 6*d* transition metals, we also calculated the bulk properties of 4*d* metals. The theoretical equilibrium Wigner-Seitz radii (w) and bulk moduli (B) are shown in Fig. 1 as a function of the periodic-table group. Good

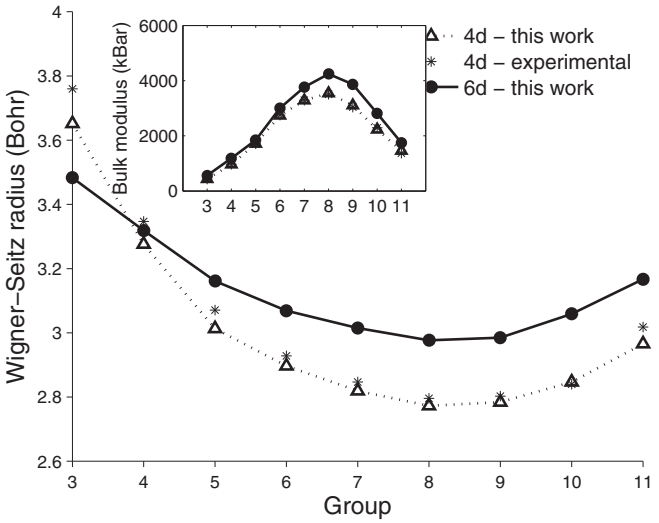

FIG. 1. Equilibrium bulk properties of 4*d* and 6*d* transition metals calculated for the ground-state crystal structures. (Main figure) Wigner-Seitz radii of 4*d* and 6*d* transition metals. (Inset) Bulk moduli for the 4*d* and 6*d* transition metals. For the 4*d* metals, the experimental data[17] are also shown (stars).

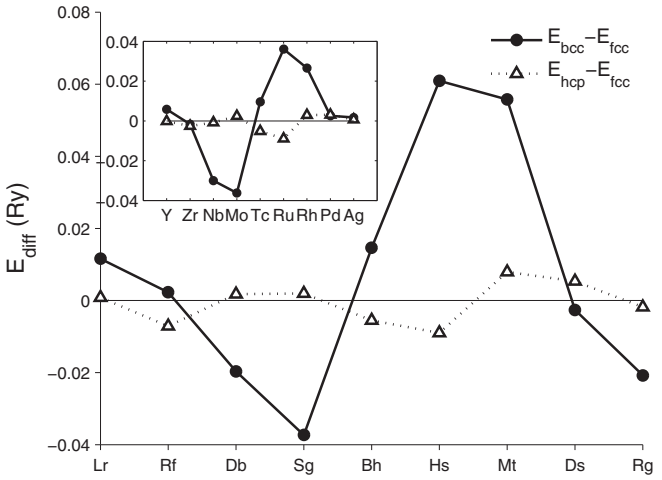

FIG. 2. (Main figure) Total energies of the bcc (closed symbols) and hcp (open symbols) structures relative to that of the fcc structure for the 6*d* metals. (Inset) Energy differences for the 4*d* metals. For both series, the SR approximation was used.

correspondence between the calculated and the measured[17] bulk properties of 4*d* metals confirms the accuracy of our calculations. The small underestimation of the equilibrium volume for some of the 4*d* metals is due to the LDA employed in the present Brief Report.[15] We observe that the bulk parameters of the 6*d* metals follow a similar trend as those of the 4*d* metals: The lowest equilibrium volume (largest bulk modulus) corresponds to Hs (Ru). The early 6*d* metals possess rather similar Wigner-Seitz radii and bulk moduli as the early 4*d* metals, whereas, the middle and late 6*d* metals have about a 10% (20%) larger Wigner-Seitz radius (bulk modulus) than the corresponding 4*d* elements. The nearly parabolic Wigner-Seitz radius (bulk modulus) versus the *d* occupation obtained for the 6*d* series can be understood from the Friedel model of cohesion in transition metals.[18] According to this model, the maximum of the cohesion energy is realized for the half-filled *d* band, and this is reflected by the maximum of the bulk modulus and the minimum of the equilibrium volume.

The structural energy differences for the 4*d* and 6*d* metals are plotted in Fig. 2 using the fcc total energy as the reference level. For the 4*d* metals (inset), the expected hcp-bcc-hcp-fcc sequence is correctly predicted by the theory. The characteristic double-peak behavior of the bcc curve can also be noted. The two bcc metals (Nb and Mo) are clearly more stable in the bcc phase than in the fcc or hcp phases. On the other hand, the last two fcc metals (Pd and Ag) turn out barely to be stable in the fcc phase: the corresponding bcc-fcc (hcp-fcc) structural energy differences being less than 2 mRy (1 mRy) for Ag. We would like to point out the good parallelism between the present results for the 4*d* metals and those obtained by the linear muffin-tin orbitals method.[4] The topology of the structural energy difference curves for the 6*d* metals is the same as that for the 4*d* metals. However, there is a striking difference, namely, that the last two 6*d* elements (Ds and Rg) are predicted to be stable in the bcc structure rather than in the fcc structure, as happens for the lighter late transition metals. That is, the noble 6*d* metals turn out to have the bcc crystallographic phase.

To find a reason for the above anomalous behavior at end of the 6*d* series, we perform additional calculations using the NR limit. For roentgenium, this gives an energy difference of $E_{\rm bcc} - E_{\rm fcc} = +1$ mRy, compared to -21 mRy obtained

TABLE I. The 6*d* transition metals. Shown are the atomic number, the chemical symbol, the electronic configuration, the half-life, and the name. The electronic configuration is given with the initial [Rn]$5f^{14}$ suppressed. The half-lives are taken from Ref. 9.

Chemical symbol	Electronic configuration	Half-life	Name
$_{103}$Lr	$6d^1 7s^2$	3.6 h	Lawrencium
$_{104}$Rf	$6d^2 7s^2$	75.5 s	Rutherfordium
$_{105}$Db	$6d^4 7s^1$	16 h	Dubnium
$_{106}$Sg	$6d^5 7s^1$	21 s	Seaborgium
$_{107}$Bh	$6d^6 7s^1$	17 s	Bohrium
$_{108}$Hs	$6d^7 7s^1$	14 s	Hassium
$_{109}$Mt	$6d^8 7s^1$	0.72 s	Meitnerium
$_{110}$Ds	$6d^9 7s^1$	7.6 s	Darmstadtium
$_{111}$Rg	$6d^9 7s^2$	3.6 s	Roentgenium

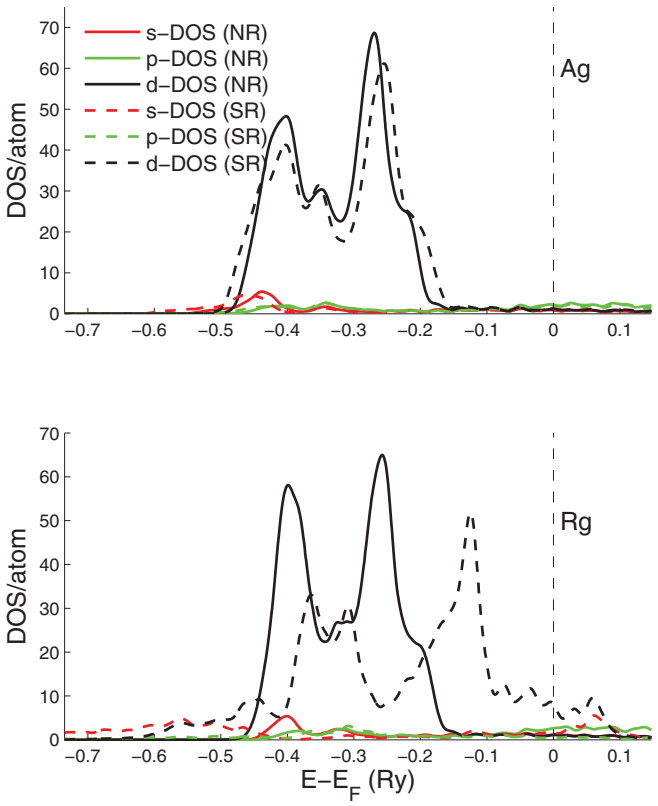

FIG. 3. (Color online) (Upper panel) DOS for silver in the bcc structure. (Lower panel) DOS for roentgenium in the bcc structure. NR (solid line) and SR (dashed line) approximations were used. s DOS (red, dark gray), p DOS (green, light gray), and d DOS (black) are shown.

in the SR approximation (Fig. 2). Thus, in the NR limit, the fcc lattice is predicted to be the most stable of the two cubic structures, in agreement with the other noble metals in group 11. We mention that the bcc-fcc structural energy difference for Ag changes in the sub-mRy level when switching off the SR terms. For a qualitative explanation for the disclosed large impact of the mass-velocity and Darwin terms, we investigate the DOS (Fig. 3, lower panel) calculated at the equilibrium volume of bcc roentgenium, using both the NR and the SR limits. The most prominent difference between the two electronic structures is that the d DOS crosses the Fermi level E_F when the SR terms are included. This gives an increase in the DOS at the Fermi level, from $D(E_F)_{\mathrm{NR}} = 5.9$ to $D(E_F)_{\mathrm{SR}} = 11.8$. The DOS increase is accompanied by a substantial increase in the interstitial electron density. To get an estimate of the charge density in the interstitial region, we

TABLE II. Number of d and s states at the Fermi level and multipole moment Q_{40}.

NR	d	s	Q_{40}	SR	d	s	Q_{40}
fcc Rg	9.656	0.689	0.028	fcc Rg	9.060	1.223	0.029
bcc Rg	9.650	0.693	0.030	bcc Rg	8.967	1.300	0.034
fcc Ds	8.794	0.584	0.033	fcc Ds	8.030	1.085	0.040
bcc Ds	8.807	0.583	0.036	bcc Ds	8.014	1.147	0.046

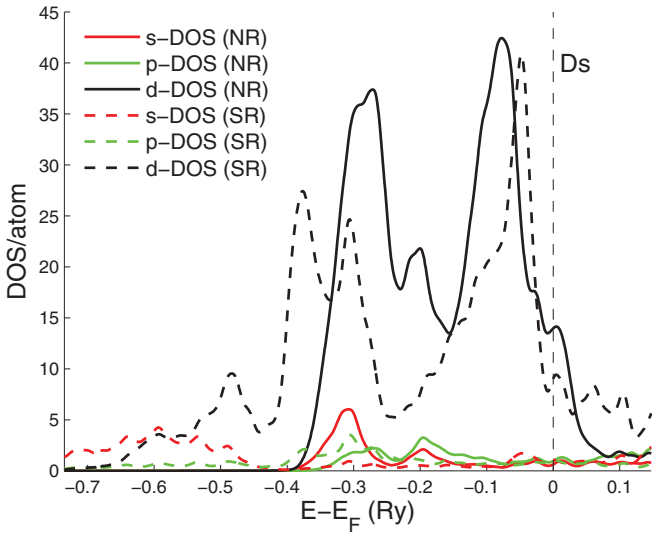

FIG. 4. (Color online) DOS for darmstadtium in the bcc structure. NR (solid line) and SR (dashed line) approximations were used. s DOS (red, dark gray), p DOS (green, light gray), and d DOS (black) are shown.

have tabulated the the first nonzero multipole moment Q_{40} of the charge density $n(\mathbf{r})$ in Table II, where $Q_{\ell m}$ is defined as

$$Q_{\ell m} = \frac{\sqrt{4\pi}}{2\ell+1} \int \left(\frac{r}{w}\right)^{\ell} n(\mathbf{r}) Y_{\ell m}(\theta,\phi) d\mathbf{r} - Z\delta_{0,0},$$

with integration performed over the Wigner-Seitz cell ($Y_{\ell m}$ stand for the real harmonics, and Z stands for for the nuclear charge). As can be seen, the interstitial density and, thus, the multipole moment increase when the SR terms are switched on. An explanation for the above trend can be found in the electron transfer from the d states to the relativistically contracted s states arising from the induced sd hybridization. As more electrons are transferred into the s states, the interstitial density is increased, since the s electrons have a larger spatial extent than the d electrons. Larger interstitial density, in turn, leads to larger Madelung interaction, which favors the bcc structure against the fcc one. The d and s occupations for different structures of Rg are listed in Table II. Indeed, it is found that the SR terms induce the d-s charge transfer. In mercury, a similar argument has been proposed to make the fcc lattice stable compared to the hcp lattice, but there, the charge transfer is from s to p states, favoring a more covalent type of bonding.[19]

As a comparison, in Fig. 3 (upper panel), we also show the DOS for bcc silver, the corresponding $4d$ element in group 11, in the NR and SR limits. In this case, the band broadening caused by the SR effects is not enough to force the d part of the DOS to cross the Fermi level, and silver has its usual sp-conduction-electron behavior. For an assessment of the relativistic effects on the DOS for the other group-11 metals using a full-potential local-orbitals method, the reader is referred to Ref. 20.

Additional calculations were also performed for the group-10 element darmstadtium, giving an energy difference of $E_{\mathrm{bcc}} - E_{\mathrm{fcc}} = +1$ mRy in the NR limit to be compared with -3 mRy in the SR limit. Hence, in this case, the SR terms stabilize the bcc structure as well. The DOS for darmstadtium

in different relativistic limits can be found in Fig. 4. As seen, the d-structured part crosses the Fermi level both in the NR and in the SR limits, indicating that the d electrons are delocalized and that electron transfer from d to s states is possible in the same way as for roentgenium. Investigating the number of states at the Fermi level for Ds (Table II), one can note that the s occupation increases while the d states decrease as the SR terms are taken into account.

To further gauge the effects of relativity, we also considered the effect of SO coupling by making calculations in the FR limit. The SO coupling has been predicted to alter the structural stability in polonium,[21] and thus, it might have a marked effect for the 6d transition metals as well. The SO term does not change the stability of the bcc phase, giving an energy difference of $E_{\mathrm{bcc}} - E_{\mathrm{fcc}} = -20$ mRy, compared to -21 mRy obtained for SR. In the case of darmstadtium, the energy difference changes from $E_{\mathrm{bcc}} - E_{\mathrm{fcc}} = -3$ mRy in the SR limit to $+1$ mRy in the FR treatment. Thus, within the present error bar, the fcc and bcc phases of Ds have similar total energies.

To conclude, we have investigated the structural stability of the 6d transition metals, finding anomalous behavior in the structure sequence, which was not expected from the established theories. The reason is found to be the SR terms, which provide a major change in the interstitial charge density. In the case of elements 110 and 111, this change is enough to make the Madelung interaction play a larger part than it does in the lighter group-10 and group-11 metals, respectively. That relativistic effects, such as SO coupling, can make a metal favor one structure over another is not very common (one example being the simple cubic polonium).[21] On the other hand, the fact that the SR terms can induce structural changes in high-symmetry metals has to the authors knowledge not been found anywhere else. Our findings suggest that further studies on heavy elements could be an interesting endeavor to perform, since results might be obtained that place established theories under a new light.

The Swedish Research Council, the Swedish Foundation for International Cooperation in Research and Higher Education (STINT), and the Hungarian Scientific Research Fund (research Project No. OTKA 84078) are acknowledged for financial support, as is Stephan Schoenecker for helpful discussions.

*ostli@kth.se

[1] P. Hohenberg and W. Kohn, Phys. Rev. **136**, B864 (1964).
[2] W. Kohn and L. J. Sham, Phys. Rev. **140**, A1133 (1965).
[3] P. Söderlind, R. Ahuja, O. Eriksson, J. M. Wills, and B. Johansson, Phys. Rev. B **50**, 5918 (1994).
[4] H. L. Skriver, Phys. Rev. B **31**, 1909 (1985).
[5] P. Söderlind, O. Eriksson, B. Johansson, J. M. Wills, and A. M. Boring, Nature (London) **374**, 524 (1995).
[6] N. Gaston, I. Opahle, H. W. Gäggeler, and P. Schwerdtfeger, Angew. Chem., Int. Ed. **46**, 1663 (2007).
[7] J. Noffsinger and M. L. Cohen, Phys. Rev. B **81**, 073110 (2010).
[8] A. Hermann, J. Furthmüller, H. W. Gäggeler, and P. Schwerdtfeger, Phys. Rev. B **82**, 155116 (2010).
[9] L. R. Morss, N. M. Edelstein, and J. Fuger, *The Chemistry of the Actinide and Transactinide Elements*, edited by L. R. Morss, N. M. Edelstein, and J. Fuger (Springer, Dordrecht, 2010), Vol. 3.
[10] O. K. Andersen, O. Jepsen, and G. Krier, in *Lectures on Methods of Electronic Structure Calculations*, edited by V. Kumar, O. K. Andersen, and A. Mookerjee (World Scientific, Singapore, 1994), pp. 63–124.
[11] L. Vitos, Phys. Rev. B **64**, 014107 (2001).
[12] L. V. Pourovskii, A. V. Ruban, L. Vitos, H. Ebert, B. Johansson, and I. A. Abrikosov, Phys. Rev. B **71**, 094415 (2005).
[13] Test calculations also were performed using the ELK code (http://elk.sourceforge.net/) and the RSPT code, J. M. Wills *et al.*, *Electronic Structure and Physical Properties of Solids: The Uses of the LMTO Method* (Springer-Verlag, Heidelberg, 2010), and similar conclusions could be reached.
[14] J. P. Perdew and Y. Wang, Phys. Rev. B **45**, 13244 (1992).
[15] M. Ropo, K. Kokko, and L. Vitos, Phys. Rev. B **77**, 195445 (2008).
[16] A. E. Kissavos, L. Vitos, and I. A. Abrikosov, Phys. Rev. B **75**, 115117 (2007).
[17] D. A. Young, *Phase Diagrams of the Elements* (University of Chicago Press, Chicago, 1991).
[18] J. Friedel, in *The Physics of Metals*, edited by J. M. Ziman (Cambridge University Press, Cambridge, UK, 1969), p. 494.
[19] P. P. Singh, Phys. Rev. Lett. **72**, 2446 (1994).
[20] H. Eschrig, M. Richter, and I. Opahle, in *Relativistic Electronic Structure Theory*, edited by P. Schwerdtfeger (Elsevier, 2004).
[21] B. I. Min, J. H. Shim, M. S. Park, K. Kim, S. K. Kwon, and S. J. Youn, Phys. Rev. B **73**, 132102 (2006).